CONFERENCE PRE-PRINT

CRYOPUMP AND FUELLING LOCATION IMPACTS ON UPSTREAM DENSITY AND DETACHMENT ON MAST-U

Q. Xia UKAEA (United Kingdom Atomic Energy Authority) Culham Campus, Abingdon, UK Email: qian.xia@ukaea.uk

D. Moulton, J.R. Harrison, H.J. Sun, N. Osborne, and the MAST Upgrade team** UKAEA Culham Campus, Abington, UK

Abstract

A cryopump was installed in the MAST-U lower divertor at the start of its fourth scientific campaign (MU04) to enhance density control, detachment front management, and impurity removal, while expanding the operational space to lower-density regimes. The tightly baffled divertor chamber quasi-isolates the divertor neutral environment from the main chamber, enabling localised neutral pressure (p_n) tuning via divertor fuelling and cryopump operation, with minimal impact on upstream plasma density. MU04 L-mode experiments and SOLPS simulations demonstrate that activating the cryopump reduces subdivertor p_n by up to 50%, while maintaining line-averaged density (\bar{n}_e) and midplane p_n . The D₂ fuelling efficiency from divertor is low (5% of neutrals reach the separatrix), resulting in weak scaling between separatrix density $(n_{e,sep})$ and divertor p_n , consistent with other devices. In contrast, main chamber fuelling (40% efficiency) yields stronger scaling (exponent > 0.6). The cryopump facilitates lower divertor p_n , aiding plasma attachment and pushing the detachment front closer to the target. Modelling indicates a 40% – 60% increase in upstream density for rollover onset in SXD, enabling a broader operational scan from attached to radiative collapse regimes. These findings validate the cryopump's role in enhancing MAST-U operational flexibility.

1. INTRODUCTION

Magnetic confinement fusion devices require precise control of plasma parameters to regulate heat and particle fluxes to divertor targets. Effective control is required to ensure efficient power exhaust and protect plasma-facing components to extend component lifetime. The Mega Ampere Spherical Tokamak-Upgrade (MAST-U) provides a unique platform to explore advanced divertor geometries, e.g., Conventional Divertor (CD) and Super-X Divertor (SXD) configurations. These geometries are designed to enhance power and particle exhaust handling, optimize detachment control, and suppress impurity penetration into the confined plasma [1,2]. Understanding the influence of these divertor configurations on neutral–plasma interactions in the scrape-off layer (SOL) and upstream electron density is essential for developing operational strategies for next-generation fusion devices such as ITER, DEMO, and STEP, where divertor performance directly impacts plasma stability and device durability [3,4].

Previous MAST-U studies have demonstrated the benefits of the SXD configuration in reducing target heat fluxes through extended connection length, flux expansion, and improved neutral trapping. However, they also make it challenging to access the attached regime in SXD. Recently, a new cryopump was installed in the lower subdivertor to regulate the detachment front and achieve attached conditions in SXD by reducing neutral density in the divertor chamber. In addition, its operation can be coupled with different fuelling locations, including high-field side (HFS), low-field side (LFS), and divertor (DIV) fuelling, to expand the accessible operational regime.

A comprehensive assessment of these effects requires the integration of experimental data with predictive modelling. Numerical tools such as the SOLPS-ITER code provide a self-consistent treatment of plasma transport, neutral dynamics, and plasma–surface interactions, enabling quantitative predictions of divertor performance under varying fuelling and cryopumping scenarios. Such integrated approaches are critical for developing physics understanding and exploring control strategies relevant to future reactor-scale devices.

In this work, we investigate fuelling efficiency and detachment front control in MAST-U using SOLPS-ITER simulations of discharges #45469 (CD) and #46860 (SXD) from the MU02 campaign. The simulations are

validated against experimental data from the subsequent MU03 and MU04 campaigns. With 1.6 MW input power and fuelling from HFS, LFS, or divertor, we evaluate the combined effects of fueling position and cryopumping on upstream electron density and detachment front changes in the divertor chamber. These results provide new insights for optimising divertor designs and fuelling strategies for future fusion reactors.

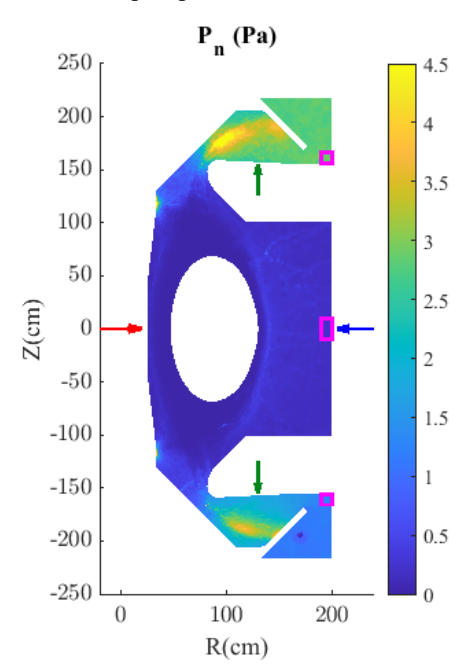
2. SIMULATION SETUP

In this work, we used the SOLPS-ITER code, which couples the multi-fluid plasma code B2.5 with the Monte-Carlo neutral code EIRENE [5]. To simplify the problem, we set up perfectly up-down symmetric double-null configurations with all the drift terms switched off.

The CD magnetic equilibrium was taken from shot #45469, and the SXD equilibrium was taken from shot #46860 at both 450ms from the MU02 campaign, using the same simulation setup as for previous L-mode MAST-U studies [6,7]. Simulations were performed with an input power of 1.6 MW, which matches the power crossing the last closed field lines with the current ohmic + NBI heating power capability on MAST-U.

We mainly fuelled with deuterium molecules from three different locations: the high-field side (HFS) midplane, the low-field side (LFS) midplane, or two up-down symmetric valves on divertor walls, as shown in Fig. 1. The fuelling rate varied between $4.3 \times 10^{21} D_2/s$ and $2.3 \times 10^{22} D_2/s$ in the major part of this paper for clarification and numerical stability.

The turbopumps were activated with a total pumping speed of 10.7 m³/s as calculated experimentally [8]. The



diffusion coefficients of the plasma in L-mode are consistent with those used in previous SOLPS simulations on MAST-U [6], which were set to match the decaying length at the outboard midplane and the heat flux profiles on targets in the shot. The diffusion coefficients in H-mode are calibrated using the same approach (Lee in preparation). A recycling coefficient of 99.9% at the targets and side walls was set to match the experimental dependence of puffing rate on upstream density.

The neutral pressure (P_n) is monitored by different fast ion gauges (FIGs) on MAST-U, which are located on the wall of the low-field side (LFS) midplane, and in the upper and lower divertors. Although the FIGs in the divertor are located outside of the simulation domain, we chose to approximate them as being inside the magenta rectangle boxes, as close to the FIGs as possible (Fig. 1).

Fig. 1. Fuelling locations marked by arrows: HFS(red), LFS(blue) and divertor (DIV, two green arrows). The background neutral pressure profile is derived from an SXD simulation. Neutral pressure is measured at three locations (magenta boxes).

3. RESULTS

3.1. Fuelling efficiency

In the MU03 campaign, experiments demonstrated that divertor fuelling ducts are less efficient than main-chamber fuelling. For example, discharges #49407 (with LFS fuelling only) and #49281 (dominated by divertor fuelling) both had similar neutral beam injection (NBI) power 1.5-1.7 Mw, with about 1 MW crossing the LCFS as measured by the bolometer. The evolutions of fuelling rates and line-averaged densities (\bar{n}_e) are presented in Fig. 3 as functions of time. Discharge #49407 solely used LFS fuelling during the whole experiment. In contrast, #49281 started with constant LFS fuelling until 0.45s, and then the chamber puffing was reduced to minimal values required for plasma stability. Meanwhile, the divertor fuelling was turned on (Fig. 3a). By ~0.57 s, divertor fuelling had become the dominant source. Note that the selected periods 0.4s to 0.8s were not in the plasma rampup phase. Instead, the slowly increasing densities, etc., indicated plasmas were in quasi-steady states. The evolution of upstream electron densities, represented by \bar{n}_e , are shown in Fig. 3b. Though the LFS-fuelling case

had a smaller total fuelling rate than divertor fuelling cases, the \bar{n}_e clearly increased much faster in the LFS fuelling discharge #49407.

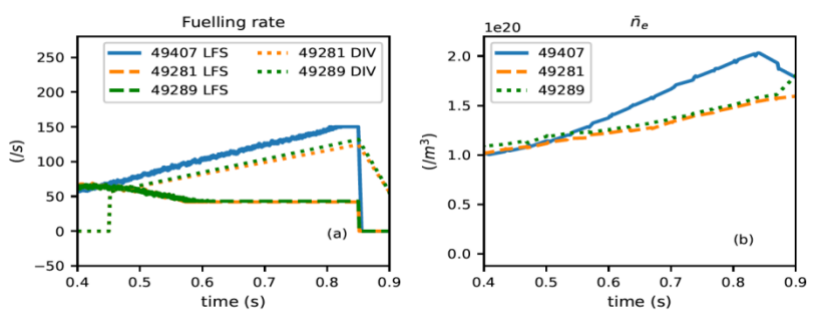


Fig. 2. (a) Fuelling rates from various ducts and (b) line-averaged electron densities for experiments #49407 and #49281 during the MU03 campaign.

To compare fuelling efficiency across different locations, the first step is to evaluate how many puffed neutrals reach the closed-field-line region and become ionised. The fuelling efficiency here is defined as

$$\frac{Sp_{puff}}{Fuel} = \frac{puffed \ neutrals \ ionised \ in \ the \ core}{total \ fuelling \ rate}.$$
 (1)

Fig. 3a summarises the results as functions of upstream electron density for all simulations. Main-chamber fuelling, including high-field-side (HFS) and low-field-side (LFS) puffing, achieves efficiencies of 10–50%, with HFS fuelling exceeding 20% in both L-mode and H-mode.

In contrast, the efficiency drops further when fuelling is shifted into the baffled divertors (divertor fuelling). A complementary perspective is provided in Fig. 3b, which evaluates the fraction of core ionisation directly from puffed neutrals:

$$\frac{\mathit{Sp}_{puff}}{\mathit{Sp}_{core}} = \frac{\mathit{puffed neutrals ionised in the core}}{\mathit{total ionised neutrals in the core}}.$$
 (2)

This metric clearly distinguishes main-chamber fuelling from divertor fuelling: Main-chamber puffing supplies more than 50% of the core plasma fuel, whereas divertor fuelling only contributes less than 40%. In the latter case, most of the ionised neutrals in the core originate from recycling and wall reflection rather than puffed neutrals.

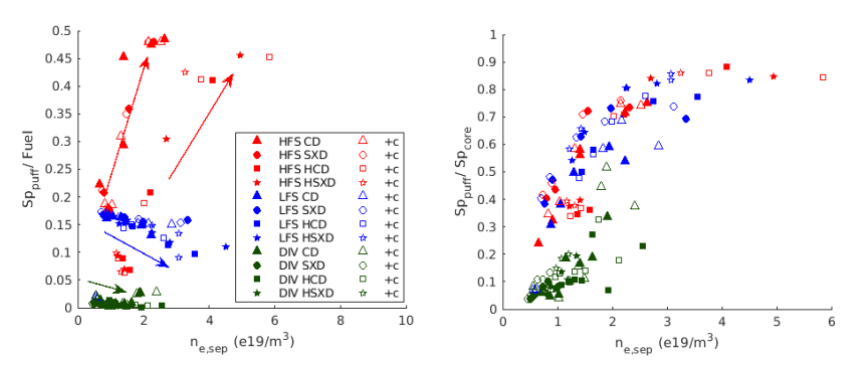


Fig. 3. Fuelling efficiency scans for CD and SXD configurations in both L-mode and H-mode (HCD or HSXD), with the lower cryopump switched Off or On (+c): Fraction of puffed neutrals ionised on closed field lines, relative to (a) the total fuelling rate, (b) the total neutrals ionised in the core region.

The lower fuelling efficiency associated with divertor fuelling on MAST-U is due to the strong isolation of the divertor chamber. In both simulations and experiments, the upstream electron densities on the outer midplane, $n_{e,sep}$, has a weak scaling correlation with the subdivertor neutral pressure P_n as demonstrated in Fig. (4a, 4b). The P_n values measured by FIGs are generally lower than those predicted in simulations, likely because the FIGs are located outside the simulated domain. An exponential fit gives: $n_{e,sep} \propto P_n^{0.3-0.34}$, which aligns with measured results on other devices [9,10]. This weak dependence on P_n suggests that the upstream density is relatively insensitive to the neutral pressure in the baffled divertor on MAST-U when fuelling from the divertor. Although

the scaling factor is influenced by fuelling locations, it remains comparable between CD and SXD configurations. In contrast to divertor fuelling, gas puffing from the main chamber is much more efficient at raising upstream density on MAST-U as shown in Fig. 2. Both simulations and experiments show a much stronger scaling between $n_{e,sep}$ (also \bar{n}_e) and P_n (Fig. 4a, 4b), with the scaling exponents for main chamber fuelling exceeding 0.6. Such strong sensitivity of upstream density to the subdivertor P_n has not yet been reported on other devices.

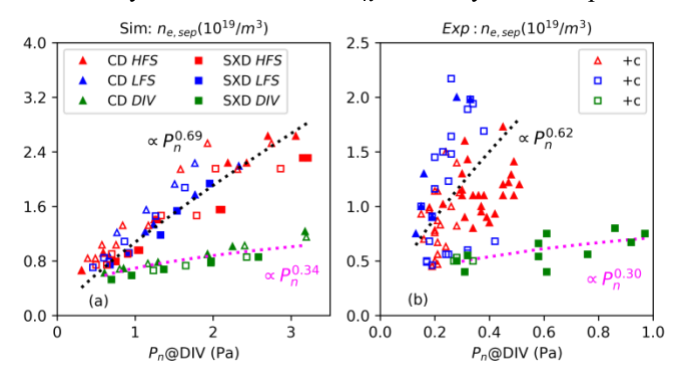


Fig. 2. Upstream electron density ($n_{e,sep}$ evaluated at the separatrix on the outboard midplane) versus neutral pressure in the divertor (P_n): (a) Data from SOLPS simulations, (b) Experimental data from multiple shots. Dashed lines represent the power-law fits for main-chamber fuelling and divertor fuelling separately.

3.2. Detachment front control

The tightly baffled divertor on MAST-U implies that the neutral environment in the divertor chamber is quasi-isolated from the main chamber [4]. We could thus use divertor fuelling (compared to HFS and LFS fuelling in the main chamber) and the cryopump to tune the neutral pressure locally in the divertor, without significantly changing the upstream neutral pressure in the main chamber. It can impact the detachment level without changing the upstream plasma conditions. As an example, Fig. 5 compares the ion sources and sinks in the lower outer divertor for two SXD discharges with different fuelling locations. For instance, selected snapshots (t = 0.53s in #46860 and t = 0.7s in #49281) correspond to the same Greenwald fraction ($f_{GW} = 0.32$). The BaSPMI analysis [11] from the line-of-sight spectroscopy system calculated the particle balance contributions from ionisation, molecular activated recombination (MAR), and electron—ion recombination (EIR).

In both discharges, the detachment fronts indicated by ionisation were located close to the X-points and almost out of the field of view, confirming that the plasmas were in a deeply detached regime. Below the detachment front, MAR dominated in the LFS fuelling shot #46860. By contrast, in the divertor fuelling shot #49281, EIR prevailed near the target, consistent with a lower divertor electron temperature. Together, these results indicate that the divertor was more detached in the predominantly divertor fuelling discharge #49281.

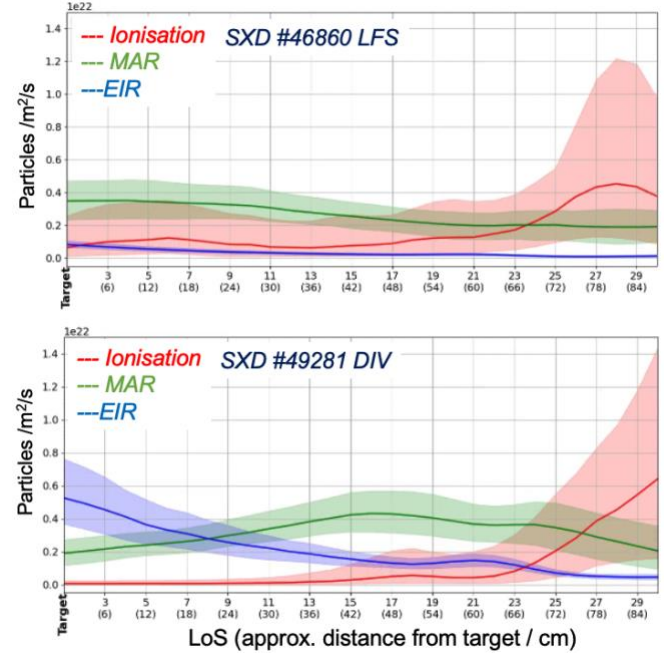


Fig. 3. Ion sources and sinks in the lower outer divertor for SXD discharges with different fuelling locations; upstream $n_{e,sep}$ matched (f_{GW} =0.32).

While divertor fuelling has been proven to increase P_n in the divertor chamber, the newly installed cryopump in the lower divertor, on the other hand, is able to locally reduce the P_n . Thus, the use of the cryopump can assist in controlling the detachment front, potentially pushing it closer to the target in both CD and SXD (Fig. 6). One challenge in the previous MAST-U campaigns was to obtain a more attached divertor (to observe the particle flux rollover clearly) in SXD configurations [6]. Because of the extended connection length and flux expansion, the particle and energy flux load on outer targets were small and the ~5eV front was typically detached from the target. Our modelling suggests the cryopump could increase the upstream density required for rollover onset by 40%-60% in SXD when it is running at the full pumping speed, as shown in Fig. (6b). This allows us to study a wider operational space, with a full scan from the attached regime to radiative collapse.

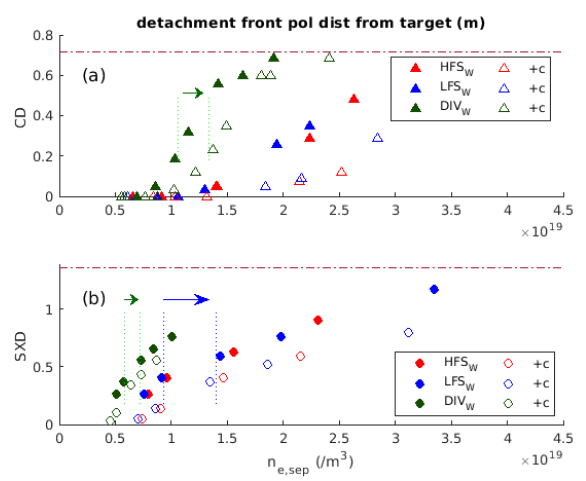


Fig. 4. Position of the 5eV detachment front in the poloidal direction as a function of the upstream separatrix electron density in (a) CD and (b) SXD configurations with the lower cryopump on or off. Dash-dotted lines mark the X-point location in the poloidal direction. Vertical dotted lines indicate the particle flux rollover onsets. The arrows show the increase in the rollover thresholds for divertor and main-chamber fuelling.

Changes in particle flux rollover onsets in simulations, as demonstrated in Fig. 6, are compared with experimental results in Fig. 7. Direct determination of $n_{e,sep}$ in experiments is less straightforward than in simulations, due to large uncertainties in locating the separatrix [12,13]. In L-mode discharges, however, \bar{n}_e is generally expected to exhibit a quasi-linear correlation with $n_{e,sep}$. For this reason, Fig. 7a and 7b show \bar{n}_e plotted against the total ion fluxes to targets ($\Sigma\Gamma_i$).

When the cryopump was activated in CD discharge #50833, the rollover threshold at the outer upper target was noticeably lower than the ones obtained at the outer lower target. (The $\Sigma\Gamma_i$ vs. \bar{n}_e at the outer upper target was similar to the discharges with cryopumping switched off. Thus, the results from shots without cryopumping are omitted here for clarity.) On the other hand, the lower cryopump enabled the outer lower target to remain attached throughout the quasi-steady phase of the shot, which could not be achieved without cryopumping. These results are consistent with expectations that the lower cryopump enhances control of detachment onset in both CD and SXD configurations.

Furthermore, Fig. 7c and 7d present the relation between $n_{e,sep}$ and $\Sigma\Gamma_i$, with $n_{e,sep}$ estimated using two-point model fits [14]. While the simulated total ion fluxes to targets are typically a factor of 2-4 higher than the experimental results at the same $n_{e,sep}$, the rollover thresholds nevertheless show good agreement between simulations and experiments. This comparison confirms that the lower cryopump has achieved its intended function of enhancing detachment control.

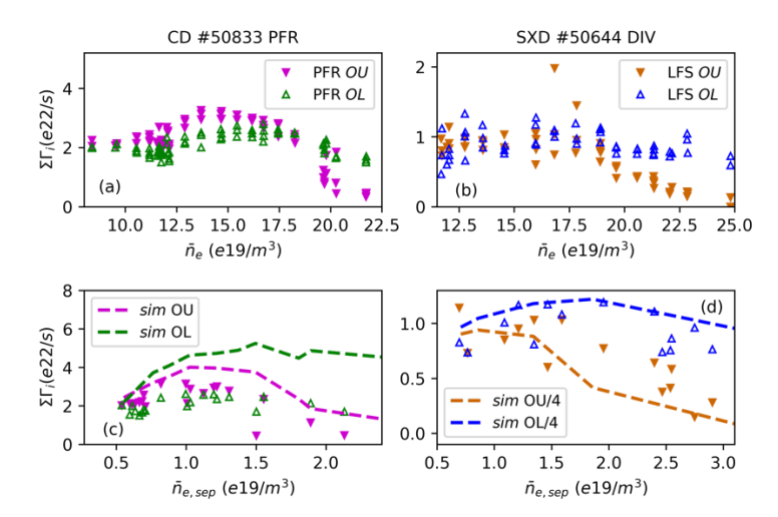


Fig. 5. (Top row) Line-averaged electron density (\bar{n}_e) as a function of total ion fluxes to the outer targets $(\Sigma \Gamma_i)$ in CD (left column) and SXD (right column) configurations. Experimental data are shown as markers. (Bottom row) Correlation between electron density at the separatrix $(n_{e,sep})$ and $\Sigma \Gamma_i$. Additional simulation results are shown as dashed lines.

3.3. Power sharing asymmetry

In addition to the outer target ion flux asymmetry presented in Fig. 7, the lower cryopump operation introduces an up-down asymmetry in heat fluxes to the upper and lower targets. The asymmetry ratio, R_{LU} , is defined as $R_{LU} = \frac{P_{lower} - P_{upper}}{P_{lower} + P_{upper}},$

$$R_{LU} = \frac{P_{lower} - P_{upper}}{P_{lower} + P_{upper}}$$

where P_{lower} and P_{upper} represent the total heat fluxes to the outer lower and outer upper targets, respectively. In the density scans presented here, which exclude drift effects, the up-down asymmetry is negligible with only wall+turbo pumping ($R_{LU} \simeq 0.0$). However, with the lower cryopump switched on, the lower target receives >50% more heat flux than the upper one, as shown in Fig.8. This asymmetry is more pronounced in the SXD compared to the CD. Furthermore, divertor fuelling cases exhibit much higher R_{LU} than main chamber fuelling cases for the same n_{e,sep}.

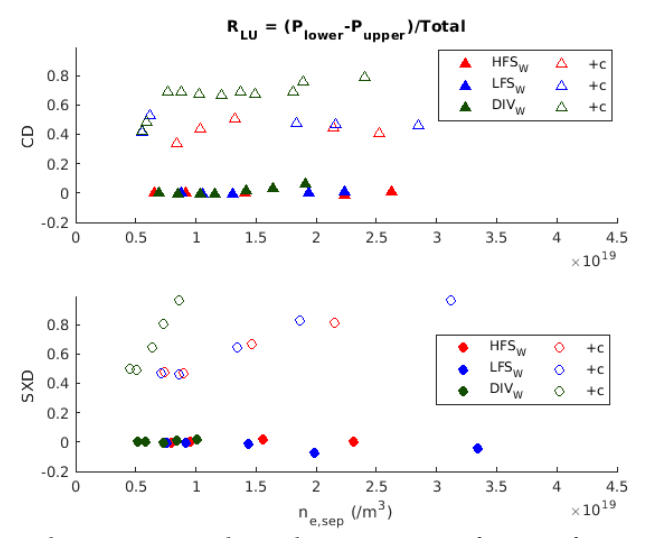


Fig. 6. Power sharing between the outer upper and outer lower targets as a function of $n_{e,sep}$ in CD and SXD configurations.

CONCLUSIONS

The installation of a cryopump in the MAST-U lower divertor has significantly enhanced operational flexibility, enabling precise control over divertor neutral pressure and detachment front position in both CD and SXD

configurations. SOLPS-ITER simulations, validated against MU03–MU04 experimental data, demonstrate that the cryopump reduces sub-divertor neutral pressure by up to 50%, and increases the upstream density of the SXD rollover threshold by 40–60%. This allows access to attached regimes in SXD and broadens the operational window from attached regime through detachment to radiative collapse.

The tightly baffled divertor chamber also highlights a clear contrast between different fuelling strategies. Divertor fuelling, with a low efficiency of ~5%, results in weak scaling of the separatrix electron density with sub-divertor neutral pressure ($n_{e,sep} \propto P_n^{0.31}$), consistent with other devices. In contrast, main chamber fuelling achieves higher efficiency (30-40%) and produces a much stronger density scaling (exponent > 0.6). The lower cryopump operation further introduces an up-down asymmetry in target heat flux sharing ($R_{LU} > 50\%$), particularly in SXD with divertor fuelling.

Together, these results validate the cryopump's role as a robust tool for regulating neutral pressure and detachment in MAST-U, while clarifying the distinct roles of divertor and main-chamber fuelling. These findings provide critical guidance for designing fuelling and exhaust strategies for future fusion reactors like ITER, DEMO, and STEP.

ACKNOWLEDGEMENTS

This work was performed using resources provided by the Cambridge Service for Data Driven Discovery (CSD3) operated by the University of Cambridge Research Computing Service (www.csd3.cam.ac.uk), provided by Dell EMC and Intel using Tier-2 funding from the Engineering and Physical Sciences Research Council (capital grant EP/T022159/1), and DiRAC funding from the Science and Technology Facilities Council (www.dirac.ac.uk).

REFERENCES

- 1. Havlíčková E, Fundamenski W, Wischmeier M, Fishpool G, Morris AW. Investigation of conventional and Super-X divertor configurations of MAST Upgrade using scrape-off layer plasma simulation. Plasma Physics and Controlled Fusion. 2014 May;56(7):075008.
- 2. Havlíčková E, Wischmeier M, Lipschultz B, Fishpool G. The effect of the Super-X divertor of MAST Upgrade on impurity radiation as modelled by SOLPS. Journal of Nuclear Materials. 2015;463:1209–13.
- 3. Asakura N, Hoshino K, Kakudate S, Subba F, Vorpahl C, Homma Y, et al. Power exhaust concepts and divertor designs for Japanese and European DEMO fusion reactors. Nuclear Fusion. 2021 Nov;61(12):126057.
- 4. Verhaegh K, Harrison J, Moulton D, Lipschultz B, Lonigro N, Osborne N, et al. Divertor shaping with neutral baffling as a solution to the tokamak power exhaust challenge. Communications Physics. 2025 May;8(1):215.
- 5. Wiesen S, Reiter D, Kotov V, Baelmans M, Dekeyser W, Kukushkin AS, et al. The new SOLPS-ITER code package. Journal of Nuclear Materials. 2015;463:480–4.
- 6. Moulton D, Harrison JR, Xiang L, Ryan PJ, Kirk A, Verhaegh K, et al. Super-X and conventional divertor configurations in MAST-U ohmic L-mode; a comparison facilitated by interpretative modelling. Nuclear Fusion. 2024 July;64(7):076049.
- 7. Verhaegh K, Harrison J, Lipschultz B, Lonigro N, Kobussen S, Moulton D, et al. Investigations of atomic and molecular processes of NBI-heated discharges in the MAST Upgrade Super-X divertor with implications for reactors. Nuclear Fusion. 2024 July;64(8):086050.
- 8. Huang J, Lisgo S, Maddison G, the MAST Team. Analysis of fuel retention on MAST by global gas balance. Plasma Physics and Controlled Fusion. 2010 June;52(7):075012.
- 9. Kallenbach A, Sun HJ, Eich T, Carralero D, Hobirk J, Scarabosio A, et al. Parameter dependences of the separatrix density in nitrogen seeded ASDEX Upgrade H-mode discharges. Plasma Physics and Controlled Fusion. 2018 Apr;60(4):045006.
- 10. Frassinetti L, Saarelma S, Verdoolaege G, Groth M, Hillesheim JC, Bilkova P, et al. Pedestal structure, stability and scalings in JET-ILW: the EUROfusion JET-ILW pedestal database. Nuclear Fusion. 2020 Nov;61(1):016001.
- 11. Verhaegh K, Harrison JR, Moulton D, Lipschultz B, Lonigro N, Osborne N, et al. Divertor shaping with neutral baffling as a solution to the tokamak power exhaust challenge [Internet]. 2024. Available from: https://arxiv.org/abs/2311.08586

- 12. Verhaegh K, Lipschultz B, Bowman C, Duval BP, Fantz U, Fil A, et al. A novel hydrogenic spectroscopic technique for inferring the role of plasma-molecule interaction on power and particle balance during detached conditions. Plasma Physics and Controlled Fusion. 2021 Jan;63(3):035018.
- 13. Berkery JW, Sabbagh SA, Kogan L, Ryan D, Bialek JM, Jiang Y, et al. Kinetic equilibrium reconstructions of plasmas in the MAST database and preparation for reconstruction of the first plasmas in MAST upgrade. Plasma Physics and Controlled Fusion. 2021 May;63(5):055014.
- 14. Pentland K, Amorisco NC, El-Zobaidi O, Etches S, Agnello A, Holt GK, et al. Validation of the static forward Grad-Shafranov equilibrium solvers in FreeGSNKE and Fiesta using EFIT++ reconstructions from MAST-U. Physica Scripta. 2025 Jan;100(2):025608.
- 15. Stagni A, Vianello N, Tsui CK, Colandrea C, Gorno S, Bernert M, et al. Dependence of scrape-off layer profiles and turbulence on gas fuelling in high density H-mode regimes in TCV. Nuclear Fusion. 2022 Aug;62(9):096031.